TOPICAL REVIEW — Topological electronic states

Topological hierarchy matters — topological matters with superlattices of defects*

Jing He(何敬)[1] and Su-Peng Kou(寇谡鹏)[2,†]

[1] Department of Physics, Hebei Normal University, Shijiazhuang 050024, China
[2] Department of Physics, Beijing Normal University, Beijing 100875, China

(Received 22 February 2016; revised manuscript received 7 April 2016; published online 28 September 2016)

Topological insulators/superconductors are new states of quantum matter with metallic edge/surface states. In this paper, we review the defects effect in these topological states and study new types of topological matters — topological hierarchy matters. We find that both topological defects (quantized vortices) and non topological defects (vacancies) can induce topological mid-gap states in the topological hierarchy matters after considering the superlattice of defects. These topological mid-gap states have nontrivial topological properties, including the nonzero Chern number and the gapless edge states. Effective tight-binding models are obtained to describe the topological mid-gap states in the topological hierarchy matters.

Keywords: defects, topological mid-gap state, topological insulator, topological superconductor

PACS: 73.21.Cd, 73.43.Cd, 71.10.Fd **DOI:** 10.1088/1674-1056/25/11/117310

1. Introduction

Topological matters including topological insulators (TIs) and topological superconductors (TSC) have become active research fields in condensed matter physics.[1,2] Topological insulators are a novel class of insulators with topological protected metallic edge states (surface states), including Chern insulators (CIs) without time reversal symmetry[3] and $Z2$ topological insulators with time reversal symmetry.[4–6] Another class of topological quantum states is topological superconductors (TSCs).[7] The Bogoliubov quasiparticles of TSCs always have a finite energy gap. Thus, the topological superconductor is a novel class of superconductors with topologically protected gapless (Majorana) edge states. According to the characterization of "ten-fold way", there are ten types of topological matters by considering the time-reversal symmetry, particle–hole symmetry, and chiral symmetry: six different types of TIs and four different types of TSCs. In addition, new types of $Z2$ TSCs beyond the ten-fold way are explored by enforcing translation invariant on the system.[8,9] By extending the topological classification of band structures to include considering the crystal point group symmetries, there may exist additional new types of topological matters — topological crystalline insulators[10] and topological crystalline superconductors. These additional symmetries lead to a non-trivial topology of bulk wave functions and gapless edge/surface states.

Topological quantum states are robust against local perturbations. From the "holographic feature" of the topological ordered states, people may use the topological defects such as the quantized vortices with half of magnetic flux $\Phi_0 = hc/2e$ and the crystal dislocations to probe the non-trivial bulk topology of the system.[11,12] In two-dimensional (2D) Chern insulators or in 2D topological superconductors, a π-flux (quantized vortex) induces mid-gap (MG) zero energy states (zero modes).[11,12] For 2D D-type topological superconductors, the Majorana fermionic zero modes localize around the quantized vortices. In addition, non-topological lattice defects (for example, vacancies) may also induce zero modes in a topological matter with spectrum symmetry.[13]

When there are two defects (quantized vortices or vacancies) nearby, the inter-defect quantum tunneling effect occurs and the fermionic zero modes on the two defects couple. For multi-topological-defect that forms a superlattice, there may exist mid-gap bands. It has been pointed out that in TIs/TSCs, for multi-vortex that forms a two dimensional superlattice on topological matters, due to the polygon rule (each Majorana/fermion gains an accumulated phase shift $|\phi| = (n-2)\pi/2$ when encircling a smallest n-polygon[14]), the defect-induced mid-gap states can be regarded as an emergent "TIs/TSCs" with nontrivial topological properties, including the nonzero Chern number and the gapless edge states.[15–17] For a topological insulator with spectrum symmetry, we also found that the vacancy-superlattice induces topological mid-gap states and the low-energy physics of the localized modes

*Project supported by the National Basic Research Program of China (Grant Nos. 2011CB921803 and 2012CB921704), the National Natural Science Foundation of China (Grant Nos. 11174035, 11474025, 11404090, and 11674026), the Natural Science Foundation of Hebei Province, China (Grant No. A2015205189), the Hebei Education Department Natural Science Foundation, China (Grant No. QN2014022), and the Specialized Research Fund for the Doctoral Program of Higher Education, China.

†Corresponding author. E-mail: spkou@bnu.edu.cn

© 2016 Chinese Physical Society and IOP Publishing Ltd

become that of an emergent "TI" on the parent TI.

In this review, we call these composite topological matters with superlattice of defects a topological hierarchy insulator or topological hierarchy superconductor. We then summarize the quantum properties of the topological hierarchy insulator and those of the topological hierarchy superconductor. In Section 2, we review the topological hierarchy superconductor induced by superlattice of quantized vortices and study the topological properties of the mid-gap states. In Section 3, we review the topological hierarchy insulators induced by superlattice of quantized vortices and those induced by the vacancy-superlattice. Finally, we give the conclusion and outlook in Section 4.

2. Topological hierarchy superconductors

In this section we will review the topological hierarchy superconductors. We take the s-wave pairing superconductor with Rashba spin–orbit (SO) coupling[15] and the $p_x + ip_y$ topological superconductor[16] as examples to show the topological properties of the topological hierarchy superconductors. For both cases, there exist mid-gap energy bands induced by flux-superlattice and the mid-gap energy bands have nontrivial topological properties including the gapless edge states and non-zero winding number. Topological tight-binding Majorana lattice models are proposed to describe the mid-gap states.

2.1. Topological hierarchy superconductor from s-wave pairing SC with Rashba SO coupling and flux-superlattice

The first example of topological hierarchy superconductor is an s-wave pairing SC with Rashba SO coupling and flux-superlattice.

The s-wave pairing SC with Rashba SO coupling on the square lattice is described by[18]

$$\mathcal{H} = \mathcal{H}_{\rm k} + \mathcal{H}_{\rm so} + \mathcal{H}_{\rm sc}, \tag{1}$$

where the kinetic term $\mathcal{H}_{\rm k}$, the Rashba SO coupling term $\mathcal{H}_{\rm so}$, and the superconducting pairing term $\mathcal{H}_{\rm sc}$ are given as

$$\begin{aligned}
\mathcal{H}_{\rm k} &= -t_{\rm s}\sum_{j\sigma}\sum_{\mu=\boldsymbol{x},\boldsymbol{y}}(c^{\dagger}_{j+\mu\sigma}c_{j\sigma}+c^{\dagger}_{j-\mu\sigma}c_{j\sigma}) \\
&\quad -u\sum_{j\sigma}c^{\dagger}_{j\sigma}c_{j\sigma}-h\sum_{j\sigma}c^{\dagger}_{j\sigma}\sigma^{z}c_{j\sigma}, \\
\mathcal{H}_{\rm so} &= -\lambda\sum_{j}\Big[(c^{\dagger}_{j-\boldsymbol{x}\downarrow}c_{j\uparrow}-c^{\dagger}_{j+\boldsymbol{x}\downarrow}c_{j\uparrow}) \\
&\quad +i(c^{\dagger}_{j-\boldsymbol{y}\downarrow}c_{j\uparrow}-c^{\dagger}_{j+\boldsymbol{y}\downarrow}c_{j\uparrow})\Big]+{\rm h.c.}, \\
\mathcal{H}_{\rm sc} &= -\Delta\sum_{j}(c^{\dagger}_{j\uparrow}c^{\dagger}_{j\downarrow}+{\rm h.c.}).
\end{aligned} \tag{2}$$

Here, $c_{j\sigma}$ ($c^{\dagger}_{j\sigma}$) annihilates (creates) a fermion at site $j = (j_x, j_y)$ with spin $\sigma = (\uparrow,\downarrow)$, $\mu = \boldsymbol{x}$ or $\boldsymbol{y}$ which is a basic vector for the square lattice, $t_{\rm s}$ is the nearest neighbor (NN) hopping parameter, λ serves as the SO coupling constant, Δ serves as the s-wave SC pairing order parameter, u is the chemical potential, and h is the strength of the Zeeman field, which is illustrated in Fig. 1(a).

Firstly, we calculate the Majorana zero mode around a single vortex by the exact diagonalization numerical approach. According to the numerical results, there exists a localized state with exact zero energy around the vortex. The zero mode is localized around the vortex core within a length-scale $\sim m^{-1}$ (m is the mass gap). For this zero mode, the fermionic-quasiparticle operator satisfies $\gamma_0 = \gamma_0^{\dagger}$, which indicates that the zero mode is indeed a Majorana fermion. When there are two vortices nearby, as shown in Fig. 1(b), the intervortex quantum tunneling effect occurs and the Majorana modes on the two vortices couple. As shown in Fig. 1(c), the energy splitting δE as a function of the distance between the two vortices D oscillates and decreases exponentially. When the two vortices are well separated, the quantum tunneling effect can be ignored and we have two quantum states with exact zero energy.[19–21]

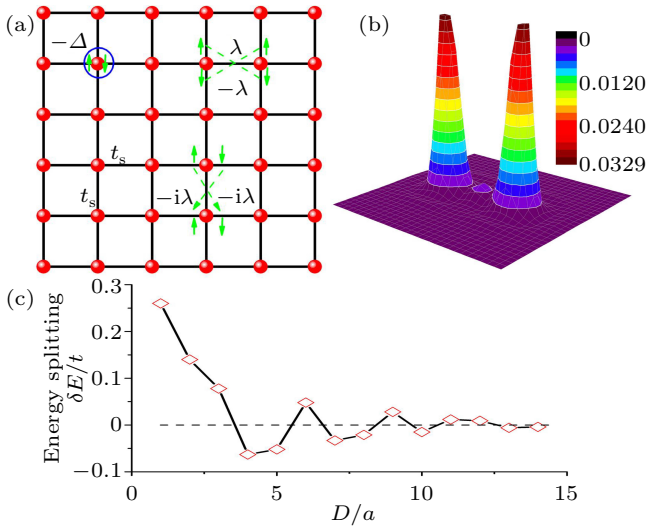


Fig. 1. (color online) (a) The illustration of s-wave pairing SC with Rashba SO coupling. (b) The particle density distribution of two zero modes around the two vortices for the case of $u = -4t_{\rm s}$, $\lambda = 0.5t_{\rm s}$, $h = 0.8t_{\rm s}$, $\Delta = 0.5t_{\rm s}$. (c) The energy splitting δE as a function of the spacial distance of the two vortices D for the case of $u = -4t_{\rm s}$, $\lambda = 0.5t_{\rm s}$, $h = 0.8t_{\rm s}$, $\Delta = 0.5t_{\rm s}$. a is the lattice constant.

Next, we numerically study the Majorana zero modes of a square flux-superlattice. The results are shown in Fig. 2(a). Because each vortex traps a Majorana fermion, we obtain a multi-Majorana fermion system for the system with the square flux-superlattice. The Majorana fermions on the square flux-superlattice will couple with each other due to the intervortex quantum tunneling effect.

The density of state (DOS) of the TSC with a square flux-superlattice is shown in Fig. 2(b). From Fig. 2(b), one can see that except for the energy bands of the paired electrons, there

exists a mid-gap energy band in the parent TSC. In particular, the mid-gap energy band has a finite energy gap. This means that this mid-gap system shown in Fig. 2(b) may be a topological state with a non-trivial topological number.

To check the topological properties of the mid-gap system, we calculate its edge states. We consider a system on a cylinder with 12 super-unitcells along x-direction while periodic boundary along y-direction. The results are shown in Figs. 2(c) and 2(d). Figure 2(c) shows that two gapless chiral edge states are localized at the boundaries. While when the parent SC is a non-topological SC, the mid-gap energy band together with the edge states disappears (see Fig. 2(d)). So the mid-gap system induced by the flux-superlattice shown in Fig. 2(a) is really a topological state.

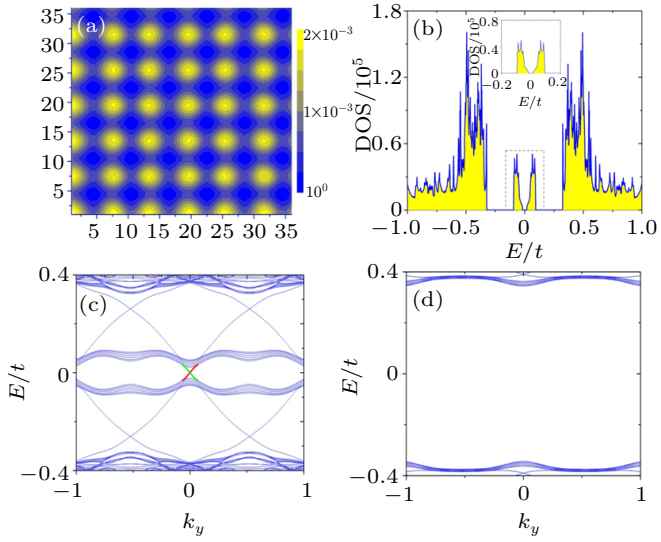


Fig. 2. (color online) (a) The illustration of vortex-lattice: the distance between two nearest vortices is $6a$. The parameters are chosen as $u=-4t_s$, $\lambda=0.5t_s$, $h=0.8t_s$, $\Delta=0.5t_s$. Each vortex traps a Majorana mode. (b) The DOS of TSC with square vortex-lattice: the mid-gap states are induced by the vortex-lattice. The inset shows the details of the mid-gap energy band. (c) The spectrum flow of TSC with square vortex-lattice on a cylinder for the case of $u=-4t_s$, $h=0.8t_s$, $\lambda=0.5t_s$, $\Delta=0.5t_s$. There exist gapless edge states. (d) The spectrum flow of non-topological SC with square vortex-lattice on a cylinder for the case of $u=-4t_s$, $h=0.8t_s$, $\lambda=0.5t_s$, $\Delta=0.5t_s$. There exist no edge states. From Ref. [15].

Then, we propose an effective tight-binding lattice model of the s-wave TSC with a square flux-superlattice, in which each vortex traps a Majorana zero mode and two Majorana zero modes couple with each other by a short range interaction. We call this effective tight-binding lattice model as the Majorana lattice model, of which the effective Hamiltonian can be written as

$$\mathcal{H}_{\mathrm{m.f}}=i\sum_{(j,k)}s_{jk}t_{jk}\gamma_k\gamma_j, \tag{3}$$

where t_{jk} is the Majorana fermion's hopping amplitude from j to k and satisfies $t_{jk}=t_{jk}^*$, and $s_{ij}=-s_{ji}$ is a gauge factor. The pair (j,k) denotes the summation that runs over all the nearest neighbor pairs (with hopping amplitude t) and all the next-nearest neighbor (NNN) pairs (with hopping amplitude t'). From the polygon rule proposed in Ref. [14], each triangular plaquette possesses $\pi/2$ quantum flux effectively. This Hamiltonian allows $Z2$ gauge choice $s_{jk}=\pm1$. From this result, we can derive that there always exists an energy gap in the Majorana lattice model as long as $t'\neq0$.

To characterize the topological properties of the Majorana lattice model, we introduce the Chern number $\mathcal{Q}$,

$$\mathcal{Q}=\frac{1}{4\pi}\iint_{\mathrm{BZ}}\mathrm{d}^2k\frac{1}{|\boldsymbol{d}(k)|^3}\boldsymbol{d}(k)\cdot\frac{\partial\boldsymbol{d}(k)}{\partial k_x}\times\frac{\partial\boldsymbol{d}(k)}{\partial k_y}, \tag{4}$$

where $\boldsymbol{d}(k)=(d_x(k),d_y(k),d_z(k))$, $d_x(k)=-2t\sin k_x$, $d_y(k)=-\sin2k_y(t+2t'\cos k_x)$, $d_z(k)=-2t\sin^2k_y+4t'\cos k_x\cos^2k_y$. In the presence of NNN hopping t', we have $\mathcal{Q}=\pm1$. Furthermore, we calculate the edge states of the Majorana lattice model and find that a gapless mode indeed exists. Now we can conclude that the (topological) Majorana lattice model captures the key low energy physics of the parent s-wave SC with a square flux-superlattice.

2.2. Topological hierarchy superconductor from topological p_x+ip_y SC with flux-superlattice

The second example of topological hierarchy superconductor is a topological p_x+ip_y SC with flux-superlattice.

Topological p_x+ip_y superconductivity is encoded in the following lattice Hamiltonian H (Fig. 3(a)):

$$\begin{aligned}H=&H_0+H_1,\\ H_0=&-t\sum_{\boldsymbol{r}}\sum_{\nu=\hat{\boldsymbol{x}},\hat{\boldsymbol{y}}}(c^\dagger_{\boldsymbol{r}+\nu}c_{\boldsymbol{r}}+\mathrm{h.c.})-u\sum_{\boldsymbol{r}}c^\dagger_{\boldsymbol{r}}c_{\boldsymbol{r}},\\ H_1=&-\frac{1}{2}\hat{\Delta}\sum_{\boldsymbol{r}}\{(c_{\boldsymbol{r}+\hat{\boldsymbol{y}}}c_{\boldsymbol{r}}-c_{\boldsymbol{r}-\hat{\boldsymbol{y}}}c_{\boldsymbol{r}})\\ &-\mathrm{i}(c_{\boldsymbol{r}+\hat{\boldsymbol{x}}}c_{\boldsymbol{r}}-c_{\boldsymbol{r}-\hat{\boldsymbol{x}}}c_{\boldsymbol{r}})\}+\mathrm{h.c.},\end{aligned}$$

where u is the chemical potential, $\hat{\Delta}$ is the electron pairing function, and t is the hopping strength. In the following parts, we set t to be the energy unit. The operator $c^\dagger_{\boldsymbol{r}}/c_{\boldsymbol{r}}$ creates/destroys an electron on lattice site $\boldsymbol{r}$ and satisfies the anti-commutation statistics $\{c_{\boldsymbol{r}},c^\dagger_{\boldsymbol{r}'}\}=\delta_{\boldsymbol{r}\boldsymbol{r}'}$.

The topological properties of the topological p_x+ip_y SC and those of the topological s-wave pairing SC with Rashba SO coupling are similar. If we do the unitary transformation

$$U=\frac{1}{\sqrt{2}}\begin{pmatrix}1&0&0&-1\\0&1&1&0\\0&-1&1&0\\1&0&0&1\end{pmatrix}$$

on the BdG Hamiltonian of the s-wave pairing SC, it will map into a p_x+ip_y SC.[22] The Rashba SO coupling corresponds to the pairing terms for the p_x+ip_y SC through the unitary transformation. Thus, the quantized vortex in p_x+ip_y SC also traps a Majorana zero mode. The energy splitting between two energy levels versus the flux-distance d oscillates and decreases exponentially, which is shown in Fig. 3(b).

We then study the $p_x + ip_y$ topological SC with a flux-superlattice. We choose $8a \times 4a$ sites to be a unit cell ($8a$ along x-direction and $4a$ along y-direction), which indicates that the flux-superlattice is anisotropy. To show the topological properties of the mid-gap spectra, we put the system on a cylinder (open boundary condition along x-direction and periodic boundary condition along y-direction). The result of this case is plotted in Fig. 3(c), which is similar to Fig. 2(c). The energy bands from the bulk consist of two kinds of fermion spectra: the Bogoliubov quasi-particles spectrum and the vortex core fermion spectrum induced by the flux-superlattice.[23] Both energy bands have energy gaps. Except for the energy bands from the bulk, there exist gapless edge states. There are two types of edge spectra: one comes from the parent topological superconductor due to its nontrivial topological properties, and the other comes from the flux-superlattice. This means that the mid-gap spectra induced by the flux-superlattice indeed have nontrivial topological properties.

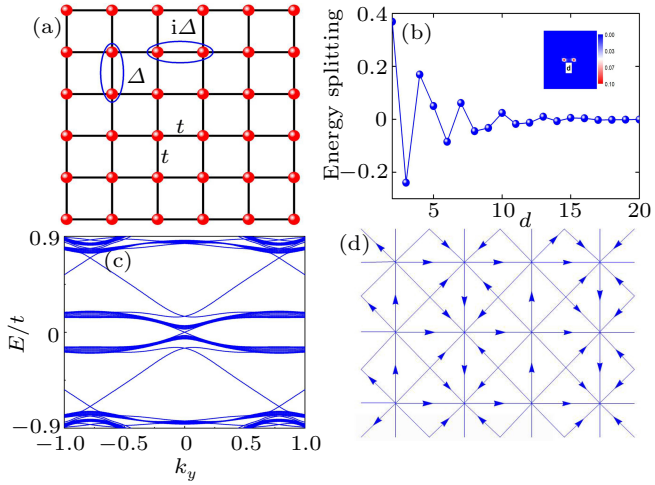


Fig. 3. (color online) (a) The illustration of topological $p_x + ip_y$ SC. (b) The energy splitting as a function of the space distance of two vortices. (c) The band structure of the topological superconductor with vortex superlattice on a cylindrical geometry. (d) The illustration of the gauge choice of the square Majorana lattice. Moving along the arrow, the fermion acquires a phase shift $\pi/2$. The accumulated phase encircling each triangular lattice plaquette anti-clockwise is $-\pi/2$. From Ref. [16].

Due to the unit cell of the vortex-superlattice is a rectangle, the effective tight-binding Majorana lattice model is given by

$$H_{\mathrm{F}} = \mathrm{i}\sum_{l}\sum_{|i-j|=l_x}\frac{t_{l_x}}{2}s_{ij}^{l_x}\gamma_i\gamma_j + \mathrm{i}\sum_{l}\sum_{|i-j|=l_y}\frac{t_{l_y}}{2}s_{ij}^{l_y}\gamma_i\gamma_j + \mathrm{i}\sum_{|i-j|=\sqrt{2}}\frac{t_{\sqrt{2}}}{2}s_{ij}^{\sqrt{2}}\gamma_i\gamma_j, \tag{5}$$

where γ_i is the operator of Majorana fermion in the i-th vortex core obeying the self-conjugate condition and the canonical commutate relation $\{\gamma_i, \gamma_j\} = 2\delta_{ij}$. The indices $l = 1, 2$ denote the nearest neighbor couplings and the next-next nearest neighbor couplings, respectively, t_{l_x} and t_{l_y} are the corresponding coupling strengths along x and y directions, and $t_{\sqrt{2}}$ is the next nearest neighbor coupling strength. Each s_{ij} connecting bond $\langle ij \rangle$ has $Z2$ gauge degree of freedom which does not affect any physical conclusions. In Fig. 3(d), we give the illustration of the gauge choice of the square Majorana lattice. Motivated by the decompose rules that two Majorana fermions fuse into a complex fermion, and no net flux through the primitive cell, we adopt the condition that there is a $\pi/2$ flux in each triangular plaquette, and the detail argument about the flux is shown in Ref. [14].

We obtain the tunneling parameters by fitting the energy dispersion of the mid-gap spectra induced by the flux-superlattice. As shown in the top panel of Fig. 4, the mid-gap spectra are obtained by a numerical approach.[23,24] The fitting dispersion of the effective tight-binding Majorana lattice model is shown in the bottom panel. We calculate the topological invariant of the effective tight-binding Majorana lattice model which gives the Chern number $\mathcal{Q} = 1$. So the effective tight-binding Majorana lattice model is a "topological SC state". This hierarchical effect has been employed to understand the topological quantum transition induced by vortex excitation in the context of Kitaev's honeycomb model supporting non-Abelian anyon excitation.[15,16,25–27] In Refs. [28] and [29], the flux-superlattice in the $p_x + ip_y$ topological SC has been studied, in which the effective tight-binding Majorana lattice model has no nontrivial topological properties.

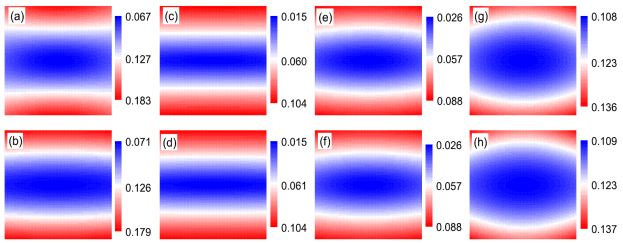


Fig. 4. (color online) Top panel: the contour plot of dispersion of mid-gap energy bands induced by vortex superlattice in $p_x + ip_y$ topological SC as a function of paired order parameter Δ in the zone $k_x \otimes k_y \in [-0.1, 0.1] \otimes [-0.2, 0.2]$. The paired order parameter is equal to 0.4, 0.8, 1.2, and 1.4 in panels (a), (c), (e), and (g), respectively. Bottom panel: the fitting dispersion of the effective tight-binding Majorana lattice model. From Ref. [16].

In the above section, we illustrate the s-wave pairing SC with Rashba SO coupling and the topological $p_x + ip_y$ SC with a square flux-superlattice. Due to the inter-vortex tunneling, there exist mid-gap energy bands induced by the flux-superlattice. We find that such mid-gap energy bands always have nontrivial topological properties including the gapless edge states and non-zero winding number. We can write down an effective tight-binding Majorana lattice model to characterize the mid-gap states and obtain the tunneling parameters by fitting the low energy spectrum with numerical calculations. Therefore, we call this type of topological superconductors with topological MG states topological hierarchy supercon-

ductors (THSC). In summary, a THSC is given by the following equation:

$$\begin{aligned}\text{THSC} &= \text{TSC} + \text{flux-superlattice} \\ &= \text{parent TSC} + \text{topological MG states}. \end{aligned} \quad (6)$$

3. Topological hierarchy insulators

In this section, we review the topological hierarchy insulators.[13,30] We take the Haldane model as an example to show the topological properties. There are two types of topological hierarchy insulators: one type is induced by a flux-superlattice, and the other is induced by a vacancy-superlattice. The first type is similar to a topological superconductor with flux-superlattice, of which the mid-gap states are described by a Majorana lattice model and can be regarded as a "topological superconductor" on the parent topological superconductor.[15,16,25] For both cases, the overlap of different zero modes around the defects leads to mid-gap states inside the band gap of the parent TI. There exist mid-gap energy bands induced by defect-superlattices and the mid-gap energy bands have nontrivial topological properties including the gapless edge states and non-zero winding number. For both cases, we use an effective tight-binding model to characterize the mid-gap states induced by the superlattice of defects.

3.1. Topological hierarchy insulators induced by flux-superlattice

Based on the Haldane model on the honeycomb lattice, we review the topological hierarchy insulator from a topological insulator with a flux-superlattice.

The Hamiltonian of the Haldane model is given by[3]

$$\hat{H}_{\text{Hal}} = -T\sum_{\langle i,j\rangle}\hat{c}_i^{\dagger}\hat{c}_j - T'\sum_{\langle\langle i,j\rangle\rangle} \mathrm{e}^{\mathrm{i}\phi_{ij}}\hat{c}_i^{\dagger}\hat{c}_j - \mu\sum_i \hat{c}_i^{\dagger}\hat{c}_i. \quad (7)$$

Here, the fermionic operator $\hat{c}_i$ annihilates a fermion on lattice site i. T is the NN hopping amplitude and T' is the NNN hopping amplitude, which are illustrated in Fig. 5(a). $\langle i,j\rangle$ and $\langle\langle i,j\rangle\rangle$ denote the NN and the NNN links, respectively. $\mathrm{e}^{\mathrm{i}\phi_{ij}}$ is a complex phase along the NNN link, and we set the direction of the positive phase $|\phi_{ij}| = \pi/2$ clockwise. μ is the chemical potential, which is set to be zero in this paper. In the following, we take the lattice constant $a \equiv 1$. The Haldane model is an integer quantum Hall insulator without Landau levels. It breaks the time reversal symmetry without any net magnetic flux through the unit cell of a periodic two-dimensional honeycomb lattice. There exists a topological invariant for the Haldane model, the Thouless–Kohmoto–Nightingale–den Nijs (TKNN) number (or the Chern number).[31] Thus, the Haldane model in Eq. (7) is a typical topological band insulator for the case of $T' \neq 0$ at half-filling.

By using the exact diagonalization numerical approach on a 72×72 lattice, we find that there exists a fermionic zero mode around each π-flux. The particle density is mainly localized around the π-flux. The length-scale of the wave-function of the zero mode is $\xi \sim v_{\text{F}}/\Delta_{\text{f}}$, where $v_{\text{F}} = 3aT/2$ is the Fermi velocity. When there are two fluxes nearby, the inter-flux quantum tunneling effect occurs and the two zero modes couple. The energy splitting δE between two energy levels versus the flux-distance L oscillates and decreases exponentially, which is shown in Fig. 5(b).

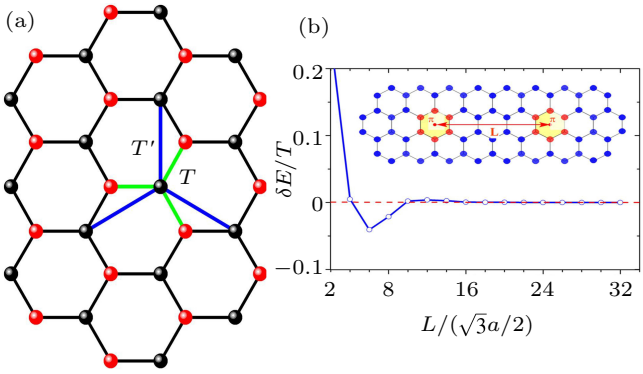


Fig. 5. (color online) (a) The illustration of Haldane model on honeycomb lattice. (b) The energy splitting δE versus the flux-distance L for the case of $T = 1.0$, $T' = 0.1$. a is the honeycomb lattice constant. The inset illustrates two π-flux with the flux-distance L. From Ref. [17].

Next we superpose a triangular flux-superlattice on the TI. By using the numerical calculations, we obtain the DOS for the Haldane model with a triangular flux-superlattice. See numerical results in Fig. 6(a) with flux-superlattice constant $L = 3\sqrt{3}a$ for the case of $T = 1.0$, $T' = 0.1$. From Fig. 6(a), one may see that the mid-gap bands appear. In Fig. 6(b), the mid-gap bands in Fig. 6(a) are zoomed in. Now, we find that there exist four points with van Hove singularity, and the mid-gap bands also have an energy gap.

To illustrate the topological properties of the mid-gap states induced by the flux-superlattice of the parent TI, we study the edge states of the TI with flux-superlattice for the case of $T = 1.0$, $T' = 0.1$. We put the Haldane model with a finite flux-superlattice along x-direction on a torus. The parent topological insulator has the periodic boundary condition along both x-direction and y-direction. While the flux-superlattice has the periodic boundary condition along y-direction and the open boundary condition along x-direction. See the numerical results in Fig. 6(c). There exist edge states along the boundaries of the flux-superlattice. The existence of the gapless zero modes on the boundary of the flux-superlattice indicates that the mid-gap system is indeed an induced "topological insulator" on the parent TI.

Finally, we also write down an effective tight-binding model to describe the mid-gap states. The quantum states of the fermionic zero mode around a π-flux can be formally described in terms of the fermion Fock states $\{|0\rangle, |1\rangle\}$. Here,

$|0\rangle$ and $|1\rangle$ denote the unoccupied state and the occupied state, respectively. These quantum states are localized around the flux within a length-scale $\xi \sim v_{\rm F}/\Delta_{\rm f}$. For the case of $\xi < L$, we can consider each flux as an isolated "atom" with localized electronic states and use the effective tight-binding model to describe these quantum states on the fluxes.

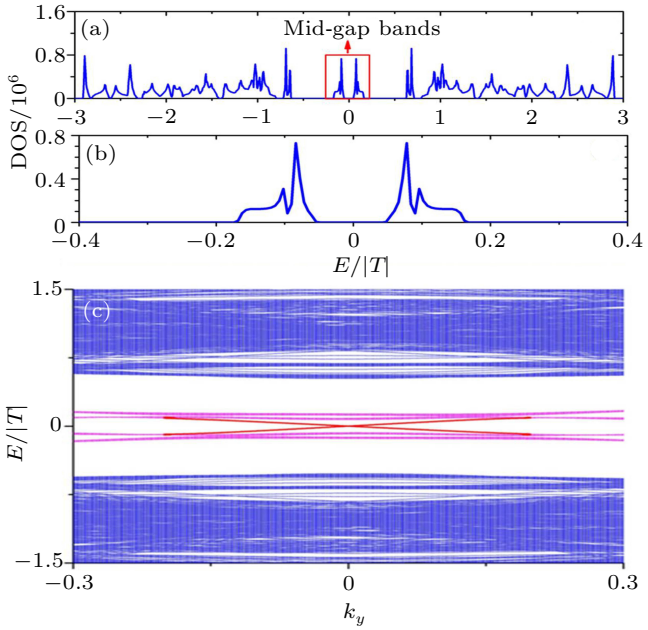


Fig. 6. (color online) (a) The DOS of TI with triangular flux-superlattice: the mid-gapped states are induced by the flux-superlattice with flux-superlattice constant $L = 3\sqrt{3}a$ in the case of $T = 1.0$, $T' = 0.1$. (b) The illustration of details of the mid-gap band in panel (a). (c) The edge states of the composite system, of which the parent Haldane model has periodic boundary along both x and y directions, and while the flux-superlattice has periodic boundary along y direction and open boundary condition along x direction. From Ref. [17].

Now, we superpose the localized states to obtain the sets of Wannier wave functions $w(R)$ with R denoting the position of the flux. Due to the formation of the triangular flux-superlattice, both the quantum-tunneling-strength δE between NN fluxes and the quantum-tunneling-strength $\delta E'$ between NNN fluxes exist. Owing to the inter-flux quantum tunneling effect, we obtain energy splitting $|\delta E_{RR'}|$, which is just the particle's hopping amplitude $|t_{RR'}|$ between two localized states on two π-fluxes at R and R'. The effective tight-binding model of the two fermionic zero modes then takes the form of $t_{RR'}\left(\hat{\alpha}_R^{\dagger}\hat{\alpha}_{R'} + \text{h.c.}\right)$ with $|t_{RR'}| = |\delta E_{RR'}|$. With considering the NN and NNN hoppings, the effective tight-binding model of the localized states around the triangular flux-superlattice is given by

$$\hat{H}_{\rm VL} = -\sum_{\langle R,R'\rangle} t_{RR'}\hat{\alpha}_R^{\dagger}\hat{\alpha}_{R'} - \sum_{\langle\langle R,R'\rangle\rangle} t'_{RR'}\hat{\alpha}_R^{\dagger}\hat{\alpha}_{R'}, \tag{8}$$

where $\hat{\alpha}_R$ is the fermionic annihilation operator of a localized state on a flux R, and $t_{RR'}$ ($t'_{RR'}$) is the hopping parameter between NN (NNN) sites R and R'. The NN (NNN) hopping term is denoted as $|t_{RR'}| = t = |\delta E|$ ($|t'_{RR'}| = |\delta E'|$). In particular, owing to the polygon rule (each fermion gains an accumulated phase shift $|\phi| = (n-2)\pi/2$ encircling around a smallest n-polygon[14]), the total phase around each plaquette of the triangular flux-lattice is $\pm\pi/2$ for fermions. The ratio between the NN hopping strength t and the NNN hopping strength t' is indeed the same as the ratio between $|\delta E|$ and $|\delta E'|$. Because people can tune $|\delta E'|/|\delta E|$ (t'/t) by changing the flux-superlattice constant L, we may regard the flux-superlattice model of the mid-gap states as an emergent controllable topological system.

Now, we study the topological properties of the effective flux-superlattice model. According to the gauge shown in Fig. 7, we choose $t_{RR'} = {\rm i}t$, $t'_{RR'} = {\rm i}t'$ if fermions hop along the directions of the arrows. Now we label the fermionic annihilation operators of the localized states on the two sub-flux-superlattices by $\hat{A}_R$, $\hat{B}_R$. By the Fourier transformation, we obtain the effective Hamiltonian of the tight-binding model of the TI with triangular flux-superlattice in momentum space as

$$\hat{H}_{\rm VL} = \sum_k \hat{\boldsymbol{\Phi}}_k^{\dagger}\mathcal{H}_k\hat{\boldsymbol{\Phi}}_k, \tag{9}$$

where $\hat{\boldsymbol{\Phi}}_k = \left(\hat{A}_k\ \hat{B}_k\right)^{\rm T}$ and $\mathcal{H}_k = (\boldsymbol{h}\cdot\boldsymbol{\tau})$ with $\boldsymbol{h} = (h_x,\ h_y,\ h_z)$ and $\boldsymbol{\tau}$ being the Pauli matrix. The three components of $\boldsymbol{h}$ are

$$\begin{aligned} h^x &= 2t\sin(\boldsymbol{k}\cdot\boldsymbol{\eta}_2) - 2t'\sin[\boldsymbol{k}\cdot(\boldsymbol{\eta}_1+\boldsymbol{\eta}_3)],\\ h^y &= -2t\cos(\boldsymbol{k}\cdot\boldsymbol{\eta}_3) - 2t'\cos[\boldsymbol{k}\cdot(\boldsymbol{\eta}_1+\boldsymbol{\eta}_2)],\\ h^z &= 2t\sin(\boldsymbol{k}\cdot\boldsymbol{\eta}_1) - 2t'\sin[\boldsymbol{k}\cdot(\boldsymbol{\eta}_2-\boldsymbol{\eta}_3)], \end{aligned} \tag{10}$$

where $\boldsymbol{\eta}_1 = L(1,\ 0)$, $\boldsymbol{\eta}_2 = L(\frac{1}{2},\ -\frac{\sqrt{3}}{2})$, $\boldsymbol{\eta}_3 = L(\frac{1}{2},\ \frac{\sqrt{3}}{2})$. In the following, for simplicity, we set the flux-superlattice constant to be $L \equiv 1$. The energy spectrums of the effective tight-binding model of the TI with triangular flux-superlattice are then obtained as

$$E_{\rm VL}(\boldsymbol{k}) = \pm|\boldsymbol{h}| = \pm\sqrt{(h^x)^2 + (h^y)^2 + (h^z)^2}. \tag{11}$$

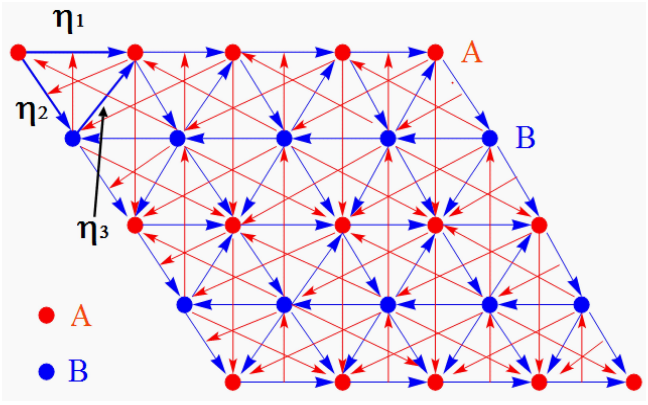


Fig. 7. (color online) The illustration of the gauge choice. Moving along the arrow (both blue arrow and red arrow), the fermion acquires a phase shift $\pi/2$. The accumulated phase encircling each triangular lattice plaquette anti-clockwise is $\pi/2$. From Ref. [17].

The topological quantum phase transition occurs when the band gap closes $E_{\rm VL}(\boldsymbol{k}) = 0$. See Fig. 8(a). We find that there exists a quantum critical point at $t'/t = 1$ that separates two quantum phases, $0 < t'/t < 1$, $t'/t > 1$. To characterize the two quantum phases, we introduce the Chern number[31]

$$C = \frac{1}{4\pi}\int \mathrm{tr}\left(\boldsymbol{n}\cdot\frac{\partial \boldsymbol{n}}{\partial k_x}\times\frac{\partial \boldsymbol{n}}{\partial k_y}\right)\mathrm{d}^2k, \tag{12}$$

with $\boldsymbol{n} = \boldsymbol{h}/|\boldsymbol{h}|$. According to the Chern number, we find that in the region of $0 < t'/t < 1$, the Chern number is 1, and in the region of $t'/t > 1$, the Chern number is -3. The tight-binding model of the TI with triangular flux-superlattice always has nontrivial topological properties. As a result, we call it topological flux-superlattice model that can describe the mid-gap states of the Haldane model with triangular flux-superlattice.

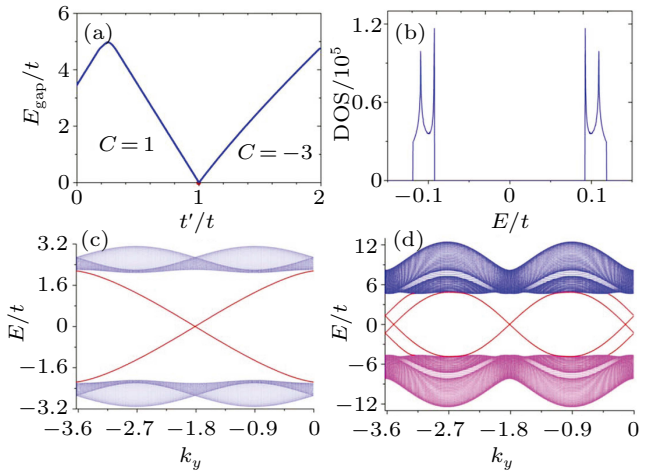


Fig. 8. (color online) (a) The topological phases versus t'/t. (b) The density of states of the free flux-lattice model. The parameters are chosen as $t/T = 0.04$, $t'/T = 0.014$. (c) The edge states of the tight-binding model of flux-superlattice for the case of $t' = 0.1t$, in which the Chern number is $C = 1$. (d) The edge states of the tight-binding model of flux-superlattice for the case of $t' = 3.1t$, in which the Chern number is $C = -3$. From Ref. [17].

In Fig. 8(b), we show the DOS of the flux-superlattice model for the case of $t/T = 0.04$, $t'/T = 0.014$. From the DOS, we can see that the effective flux-superlattice model has a finite energy gap and there exist four points with van Hove singularity. Figures 8(c) and 8(d) show the edge states for the cases of $t' = 0.1t$ (the Chern number is $C = 1$) and $t' = 3.1t$ (the Chern number is $C = -3$), respectively.

Hence, the low energy physics of the Haldane model with flux-superlattice can be described by an effective flux-superlattice model. The effective flux-superlattice model shows nontrivial topological properties, including a nontrivial topological invariant and gapless edge states. In this sense, the effective flux-superlattice model is really an emergent "topological insulator" on the parent TIs. Our results are more exotic than those in Ref. [32], in which a (non-topological) free-fermion model on a honeycomb lattice with flux-superlattice is studied.

We have studied the Haldane model with triangular flux-superlattice. Using a similar approach, we studied the Haldane model with other types of flux-superlattices such as the square flux-superlattice and honeycomb flux-superlattice, and found similar topological properties. In this sense, the topological mid-gap states always exist in a TI with flux-superlattice. In addition, we need to point out that the Kane–Mele model[5] or the spinful Haldane model[33] with flux-superlattice exhibit similar topological features. Due to the spin degree of freedom, a π-flux on these models traps two zero modes. The overlap of the zero modes also gives rise to a topological mid-gap system inside the band gap of the parent TIs. When one considers the interaction between the two-component fermions, the topological mid-gap system may lead to quite different physics consequences.

As a result, we call this type of topological insulators with topological MG states topological hierarchy insulators (THIs). In summary, THI from flux-superlattice is given by the following equation:

$$\begin{aligned}\mathrm{THI} &= \mathrm{TI} + \text{flux-superlattice}\\ &= \text{parent TI} + \text{topological MG states}.\end{aligned} \tag{13}$$

3.2. Topological hierarchy insulators induced by vacancy-superlattice

Based on the Haldane model on the square lattice, we review the topological hierarchy insulator from a topological insulator with a vacancy-superlattice.

The Hamiltonian of the (spinless) Haldane model on the square lattice is given by[3,34]

$$\begin{aligned}\hat{H}_{\rm parent} = &-t\sum_{i\in A}\left(\hat{c}^\dagger_{i+\hat{x}}\hat{c}_i + i\hat{c}^\dagger_{i+\hat{y}}\hat{c}_i + \mathrm{h.c.}\right)\\ &+t\sum_{i\in B}\left(\hat{c}^\dagger_{i+\hat{x}}\hat{c}_i - i\hat{c}^\dagger_{i+\hat{y}}\hat{c}_i + \mathrm{h.c.}\right)\\ &-t'\sum_{i\in A}\left(\hat{c}^\dagger_{i+\hat{x}+\hat{y}}\hat{c}_i + \hat{c}^\dagger_{i+\hat{x}-\hat{y}}\hat{c}_i + \mathrm{h.c.}\right)\\ &+t'\sum_{i\in B}\left(\hat{c}^\dagger_{i+\hat{x}+\hat{y}}\hat{c}_i + \hat{c}^\dagger_{i+\hat{x}-\hat{y}}\hat{c}_i + \mathrm{h.c.}\right),\end{aligned} \tag{14}$$

where $\hat{c}_i$ is the annihilation operator of the fermions at site i. A and B label the sublattices. t and t' are the nearest-neighbor and the next-nearest-neighbor hopping parameters, respectively. For the Hamiltonian in Eq. (14), there exists a π-flux in each square plaquette and a $\pi/2$-flux in each triangular lattice. The illustration of the Haldane model on the square lattice is shown in Fig. 9(a). The Haldane model on the square lattice is a TI with quantum anomalous Hall (QAH) effect. The Chern number $C_{\rm parent}$ of the (parent) Haldane model is 1 and the quantized Hall conductivity is e^2/h.

Vacancy is a non-topological defect and cannot induce a fermion zero mode when we consider a vacancy in TI. However, we have pointed out that if the Hamiltonian has the

particle–hole (PH) symmetry, then a vacancy can induce a zero mode. Under PH transformation, we have

$$\hat{H}_{\text{parent}} = -\mathcal{P}^{\dagger}\hat{H}_{\text{parent}}\mathcal{P}, \tag{15}$$

where $\mathcal{P} = \mathcal{R}\cdot\mathcal{K}$ is the PH transformation operator.[33,35] Here, $\mathcal{R}$ is an operator that leads to $\hat{c}_i \leftrightarrow (-1)^i\hat{c}_i^{\dagger}$ and $\mathcal{K}$ is the complex conjugate operator. As a result, each energy level with positive energy E is paired with an energy level with negative energy $-E$. If the Hamiltonian is on a bipartite lattice, the quantum levels of the system with a single vacancy become an odd number. As a result, there must exist an unpaired electronic state when we remove a lattice site to create a vacancy. Because of the PH symmetry, the corresponding unpaired electronic state must have exactly zero energy.[36]

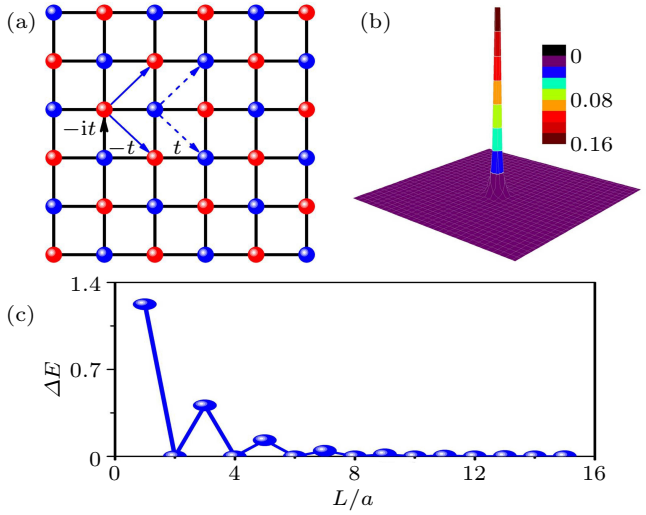


Fig. 9. (color online) (a) The illustration of the Haldane model on square lattice. Blue and red dots represent A, B sublattices. The blue arrows represent t' and the dashed blue arrows represent $-t'$. (b) The particle density distribution around the zero energy vacancy. (c) The energy splitting ΔE between two vacancies as a function of L (the distance of two nearby vacancies). The parameter is $t' = 0.2t$. From Ref. [30].

The Hamiltonian in Eq. (14) satisfies the particle–hole (PH) symmetry. So, each vacancy induces a zero mode. We have calculated the fermionic zero mode around a single vacancy by the exact diagonalization numerical approach on a 60×60 square lattice and obtain the particle density distribution around the vacancy in Fig. 9(b). The particle density is localized around the vacancy center within a length-scale $\sim(\Delta_{\text{f}})^{-1}$, where Δ_{f} is the fermion energy gap. The localization effect is similar to that of a flux on TI/TSC. We denote the wave-function of the zero mode by $\psi_0(r_i - R)$, where R is the position of the vacancy. The quantum states of the fermionic zero mode around a vacancy can be formally described in terms of the fermion Fock states $\{|0\rangle, |1\rangle\}$. Here, $|0\rangle$ and $|1\rangle$ denote the empty state and the occupied state, respectively.

We next study the Haldane model with vacancy-superlattice. When there are two vacancies nearby, the inter-vacancy quantum tunneling effect occurs and the fermionic zero modes on the two vacancies couple. The lattice constant of the vacancy-superlattice (VSL) is denoted by L, which is the distance between two nearby vacancies. When the vacancies are located on different sublattices, the energy splitting ΔE is finite (L/a is an odd number); when the vacancies are located on the same sublattice, the energy splitting vanishes, $\Delta E = 0$ (L/a is an even number). The energy splitting ΔE between two vacancies as a function of L is shown in Fig. 9(c). When two vacancies are well separated (or $L\to\infty$), the quantum tunneling effect can be ignored and we have two quantum states with exact zero energy. In contrast, for the smaller L (odd number times of a), the coupling between two zero modes becomes stronger and the energy splitting cannot be neglected.

For the case of $\xi < L$, we can consider each vacancy as an isolated "atom" with localized electronic states and use the effective tight-binding model to describe these quantum states induced by the VSL. We now construct the superpositions of the localized states to obtain the sets of Wannier wave functions $\psi_0(r_i - R)$. In general, the effective tight-binding model of the localized states induced by the VSL becomes

$$\begin{aligned}\hat{H}_{1-\text{VL}} = &-\sum_{\langle R,R'\rangle} T_{RR'}\hat{d}_R^{\dagger}\hat{d}_{R'} - \sum_{\langle\langle R,R'\rangle\rangle} T'_{RR'}\hat{d}_R^{\dagger}\hat{d}_{R'} \\ &- \sum_{\langle\langle\langle R,R'\rangle\rangle\rangle} T''_{RR'}\hat{d}_R^{\dagger}\hat{d}_{R'} + \cdots,\end{aligned} \tag{16}$$

where $\hat{d}_R$ is the fermionic annihilation operator of a localized state on vacancy R. $T_{RR'}$ ($T'_{RR'}$, $T''_{RR'}$) is the hopping parameter between NN (NNN, next next nearest neighbor (NNNN)) sites R and R' and is determined by the energy splitting ΔE, $|T_{RR'}| = |\Delta E|$ ($|T'_{RR'}| = |\Delta E'|$, $|T''_{RR'}| = |\Delta E''|$). In general, because $|T''_{RR'}| \ll |T'_{RR'}|$, $|T_{RR'}|$, we only consider the NN and NNN hopping terms. Because the parent Hamiltonian in Eq. (14) has the PH symmetry, the effective tight-binding model of the localized states induced by the VSL $\hat{H}_{1-\text{VL}}$ in Eq. (16) also has the PH symmetry,

$$\hat{H}_{1-\text{VL}} = -\mathcal{P}^{\dagger}\hat{H}_{1-\text{VL}}\mathcal{P}. \tag{17}$$

Because the energy splitting ΔE only determines the particle's hopping amplitude $|T_{RR'}|$, we need to settle down the phase of $T_{RR'}$. In particular, to preserve the PH symmetry, the total phase around a plaquette with four NN vacancies can be either π or 0. One approach is to count the total flux number inside the plaquette. For the mid-gap states induced by VSL, every four NN vacancies form an $L\times L$ square, of which the total flux number is just $L^2/2$ and the total phase around a plaquette is πL^2. After considering the compact condition, we have $0/\pi$-flux inside each plaquette if L^2 is an even/odd number. In addition, we also use a numerical approach to check the above prediction of the flux number inside the plaquette.

We then consider the Haldane model with a square-VSL and the lattice constant L set to $3a$. See the illustration in

Fig. 10(a). From the above discussion it can be seen that there exists a π-flux in each square plaquette of VSL and a $\pi/2$-flux in each triangular plaquette of VSL. From the configuration of zero modes around vacancies in Fig. 10(a), one can see that the quantum states induced by VSL can be regarded as a new generation of lattice model, of which the vacancies play the role of the "atoms".

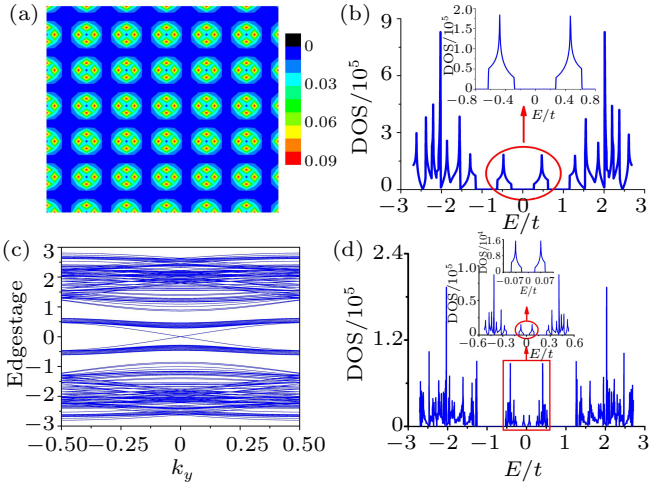


Fig. 10. (color online) (a) The illustration of square-VSLs on square lattice. (b) The DOS of the Haldane model with square-VSL for $L = 3a$: the mid-gap states are induced by the square-VSL. (c) The edge states of mid-gap states. The parameter is $t'/t = 0.2$. (d) The DOS of TFI. The insets show the DOSs of the mid-gap states. From Ref. [30].

As a result, we obtain an effective Hamiltonian that describes the vacancy-induced square lattice, written in the form

$$\begin{aligned}\hat{H}_{1-\mathrm{VL}} =& -T\sum_{R\in\bar{A}}\left(\hat{d}^{\dagger}_{R+L\hat{x}}\hat{d}_R + \mathrm{i}\hat{d}^{\dagger}_{R+L\hat{y}}\hat{d}_R + \mathrm{h.c.}\right)\\ &+ T\sum_{R\in\bar{B}}\left(\hat{d}^{\dagger}_{R+L\hat{x}}\hat{d}_R - \mathrm{i}\hat{d}^{\dagger}_{R+L\hat{y}}\hat{d}_R + \mathrm{h.c.}\right)\\ &+ T'\sum_{i\in\bar{A}}\left(\hat{d}^{\dagger}_{R+L\hat{x}+L\hat{y}}\hat{d}_R + \hat{d}^{\dagger}_{R+L\hat{x}-L\hat{y}}\hat{d}_R + \mathrm{h.c.}\right)\\ &- T'\sum_{i\in\bar{B}}\left(\hat{d}^{\dagger}_{R+L\hat{x}+L\hat{y}}\hat{d}_R + \hat{d}^{\dagger}_{R+L\hat{x}-L\hat{y}}\hat{d}_R + \mathrm{h.c.}\right), \quad (18)\end{aligned}$$

where T and T' are the effective NN and NNN hopping parameters, respectively. $\bar{A}$ and $\bar{B}$ label the sublattices of VSL. By comparing Eq. (14) with Eq. (18), one can see the corresponding relationship, $\hat{c}_i \longleftrightarrow \hat{d}_R$, $t \longleftrightarrow T$, and $t' \longleftrightarrow -T'$. For the defect-induced quantum states, the energy spectrum and DOS are obviously similar to those of the parent Hamiltonian in Eq. (14).

From the DOS of the Haldane model with square-VSL for $t'/t = 0.2$ and $L = 3a$ in Fig. 10(b), the mid-gap energy bands appear near the chemical potential. It is obvious that the MG states are induced by the VSL. In particular, we find that the mid-gap states also have an energy gap and exist two points with van Hove singularity. The DOS of the MG states is very similar to that of the parent TI. By fitting a curve to the DOS of the vacancy-induced quantum states, we obtain the effective hopping parameters as $T = 0.22t$ and $T' = 0.07t$.

To illustrate the topological properties of the Haldane model with square-VSL, we study its edge states. As a result, when the system has periodic boundary condition along y-direction but open boundary condition along x-direction, there exist the gapless edge states. On the other hand, we consider the half filling case, of which the system has zero Chern number. When the parent topological insulator has periodic boundary condition along both x-direction and y-direction, while the VSL has periodic boundary condition along y-direction but open boundary condition along x-direction, there may exist gapless edge states. See the numerical results in Fig. 10(c) for the case of $t'/t = 0.2$ and $L = 3a$, there indeed exist gapless edge states on the boundaries of VSL.

In addition, we also calculate the Haldane model on the honeycomb lattice with the honeycomb-VSL. The Haldane model on the honeycomb lattice also has the PH symmetry, and honeycomb-VSL can also induce a topological hierarchy insulator.

In general, the Haldane model with a square-VSL of odd number L^2 has nontrivial topological properties and is different from the traditional TIs. As a result, we call this type of topological insulator with topological MG states topological hierarchy insulators (THIs). In summary, THI from vacancy-superlattice is given by the following equation:

$$\begin{aligned}\mathrm{THI} &= \mathrm{TI} + \text{vacancy-superlattice}\\ &= \text{parent TI} + \text{topological MG states}. \quad (19)\end{aligned}$$

There also exist a particular type of topological hierarchy insulator, topological fractal insulator (TFI), which is a topological hierarchy insulator with infinite generations of self-similar $L\times L$-square-VSLs. To construct a TFI, we first consider a topological hierarchy insulator with self-similar MG states. Because we can tune T'/T (or $\Delta E'/\Delta E$) by changing the NNN hopping parameter t' of the parent TI or the VSL constant L, the MG states can be self-similar to the parent topological states for the case of $T/T' = t/t'$. From numerical calculations, we obtain the self-similarity case, where smaller/bigger t/t' leads to bigger/smaller T/T'. Now, under the self-similar condition $T/T' = t/t'$, the effective Hamiltonian that describes the MG states becomes

$$\hat{H}_{1-\mathrm{VL}} = \alpha\hat{H}^{*}_{\mathrm{parent}}, \quad (20)$$

where $\alpha = T/t$ ($\alpha < 1$) is an energy-scaling ratio.

Next, we regard the vacancy-induced MG states as a parent TI and introduce an additional VSL on it. Using the recursive relation, we can see that there exist additional MG states inside the energy gap of the first generation MG states (which we refer to as generation-1 MG states). Consequently, we obtain a new generation of topological MG states (we call such

MG states in the energy gap of the MG states as generation-2 MG states). Using the same procedure, we can construct a THI with n-generation MG states and eventually a THI with infinite generations of self-similar MG states that is just a TFI. Then, under the self-similar condition $T/T' = t/t'$, the effective Hamiltonian of the generation-n MG states is given by

$$\hat{H}_{n-\mathrm{VL}} = \begin{cases} \alpha^n \hat{H}_{\mathrm{parent}}, & n \text{ is an even number,} \\ \alpha^n \hat{H}^*_{\mathrm{parent}}, & n \text{ is an odd number.} \end{cases} \tag{21}$$

From the DOS in Fig. 10(d), we can see that the DOS of the MG states is always self-similar.

It is known that a self-similar object looks "roughly" the same on different scales and fractal is a particularly self-similar object that exhibits a repeating pattern displaying at every scale. The topological fractal insulator provides a unique example of topological matters with self-similarity, in which the topological properties always look the same on different energy scales (α^{2n}) or different length scales (L^{2n}).

4. Conclusion and outlook

In this review, we mainly talk about the defects induced topological states in TIs/TSCs. A new type of topological matter is defined — topological hierarchy matter. There are two types of topological hierarchy matters: one is the topological hierarchy superconductor induced by flux-superlattice, and the other is the topological hierarchy insulator induced by vacancy-superlattice or flux-superlattice. After considering the superlattice of defects, the topological mid-gap states are induced in these topological hierarchy matters. The topological mid-gap states may have nontrivial topological properties, including the nonzero Chern number and the gapless edge states. Effective tight-binding models are obtained to describe the topological mid-gap states in the topological hierarchy matters.

In the future, an important issue is to look for the topological hierarchy superconductor induced by vacancy-superlattice. For the topological hierarchy insulator, the correlation effect may be more relevant than that in the traditional correlated topological insulator. So, we will study the correlated hierarchy topological insulator and find new type quantum exotic states after considering the correlation effect. Furthermore, we try to realize topological hierarchy matters in condensed matter physics and explore their non-trivial topological properties. On the other hand, cold atoms in optical lattices are an extensively developing research field.[37–40] By using the ultracold-atom technique, we can accurately control the interaction. The cold atoms in optical lattices are an ideal experimental platform for realizing topological hierarchy matters.

References

[1] Wen X G 1990 *Int. J. Mod. Phys. B* **4** 239
[2] Wen X G 1995 *Adv. Phys.* **44** 405
[3] Haldane F D M 1988 *Phys. Rev. Lett.* **61** 2015
[4] Kand C L and Mele E J 2005 *Phys. Rev. Lett.* **95** 226801
[5] Kand C L and Mele E J 2005 *Phys. Rev. Lett.* **95** 146802
[6] Bernevig B A, Huge T L and Zhang S C 2006 *Science* **314** 1757
[7] Read N and Green D 2000 *Phys. Rev. B* **61** 10267
[8] Kou S P and Wen X G 2009 *Phys. Rev. B* **80** 224406
[9] Kou S P and Wen X G 2010 *Phys. Rev. B* **82** 144501
[10] Fu L 2011 *Phys. Rev. Lett.* **106** 106802
[11] Ran Y, Vishwanath A and Lee D H 2008 *Phys. Rev. Lett.* **101** 086801
[12] Qi X L and Zhang S C 2008 *Phys. Rev. Lett.* **101** 086802
[13] He J, Zhu Y X, Wu Y J, Liu L F, Liang Y and kou S P 2013 *Phys. Rev. B.* **87** 075126
[14] Grosfeld E and Stern A 2006 *Phys. Rev. B* **73** 201303(R)
[15] Zhou J, Wu Y J, Li R W, Kou S P 2013 *Europhys. Lett.* **102** 47005
[16] Zhou J, Wang S Z, Wu Y J, Li R W and Kou S P 2014 *Phys. Lett. A* **378** 2576
[17] Wu Y J, He J and Kou S P 2014 *Europhys. Lett.* **105** 47002
[18] Sato M, Takahashi Y and Fujimoto S 2009 *Phys. Rev. Lett.* **103** 020401
[19] Cheng M, Lutchyn R M, Galitski V and Das Sarma S 2010 *Phys. Rev. B* **82** 094504
[20] Cheng M, Lutchyn R M, Galitski V and Das Sarma S 2009 *Phys. Rev. Lett* **103** 107001
[21] Baraban M, Zikos G, Bonesteel N and Simon S H 2009 *Phys. Rev. Lett.* **103** 076801
[22] Sato M, Takahashi Y and Fujimoto S 2009 *Phys. Rev. Lett.* **103** 020401
[23] Rosenstein B, Shapiro I and Shapiro B Y 2013 *J. Phys.: Condens. Matter* **25** 075701
[24] Mel'nikov A S, Ryzhov D A and Silaev M A 2008 *Phys. Rev. B* **78** 064513
[25] Lahtinen V, Ludwig A W W, Pachos J K and Trebst S 2012 *Phys. Rev. B* **86** 075115
[26] Lahtinen V 2011 *New J. Phys.* **13** 075009
[27] Lahtinen V, Ludwig A W W and Trebst S 2014 *Phys. Rev. B* **89** 085121
[28] Biswas R 2013 *Phys. Rev. Lett.* **111** 136401
[29] Silaev M A 2013 *Phys. Rev. B* **88** 064514
[30] He J, Liang Y and Kou S P 2015 *Europhys. Lett.* **112** 17010
[31] Thouless D J, Kohmoto M, Nightingale P and Nijs M den 1982 *Phys. Rev. Lett.* **49** 405
[32] Kamfor M, Dusuel S, Schmidt K P and Vidal J 2011 *Phys. Rev. B* **84** 153404
[33] Xue Y, He J, Zhang X H and Kou S P 2015 *J. Phys.: Condens. Matter* **27** 356001
[34] Liu X L, Wang Z Q, Xie X C and Yu Y 2011 *Phys. Rev. B* **83** 125105
[35] Yang C N and Zhang S C 1990 *Mod. Phys. Lett. B* **4** 759
[36] He J, Kou S P, Liang Y and Feng S P 2011 *Phys. Rev. B* **83** 205116
[37] Greiner M, Mandel O, Esslinger T, Hänsch T W and Bloch I 2002 *Nature* **415** 39
[38] Jaksch D, Bruder C, Cirac J I, Gardiner C W and Zoller P 1998 *Phys. Rev. Lett.* **81** 3108
[39] Lewenstein M, Sanpera A, Ahufinge V, Damski B, Sen A and Sen U 2007 *Advances in Physics* **56** 243
[40] Bloch I, Dalibard J and Zwerger W 2008 *Rev. Mod. Phys.* **80** 885